RESEARCH ARTICLE

**ADVANCED
ENERGY & SUSTAINABILITY
RESEARCH**
Open Access

www.advenergysustres.com

Calcium Alginate Core–Shell Liquid Beads Encapsulated with Microalgae for Wastewater Treatment

*Du Tuan Tran, Nhat-Khuong Nguyen, Ajeet Singh Yadav, Ann Chuang, Michele Burford, Fariba Malekpour Galogahi, Kamalalayam Rajan Sreejith, and Nam-Trung Nguyen**

Liquid beads are core–shell particles with a liquid core and a solid shell. Calcium alginate liquid beads have been emerging as a promising platform for cell encapsulation. These beads have demonstrated their capability of encapsulating and culturing a wide range of human cells for tissue engineering. However, a significant research gap remains in the application of alginate liquid beads for encapsulating photosynthetic microorganisms. Herein, fast-growing microalgae strain *Chlorella vulgaris* is encapsulated into calcium alginate liquid beads to facilitate the removal of nutrients from wastewater, minimizing the risk of eutrophication. Liquid bead-microalgae systems are prepared, using different calcium ion concentrations as crosslinking ions. It has been thoroughly characterized for their morphologies, cell growth patterns, nutrient removal capabilities, and overall stability throughout the wastewater treatment process, with upflow anaerobic sludge blanket effluent as the wastewater model. The results indicate that the liquid bead-microalgae system with the highest calcium ion concentration (5%) performs more efficiently, exhibiting a well-formed crosslinking structure, leading to rapid cell growth with the highest cell density and the most effective removal of nutrients. The findings from this study provide valuable insights for future optimization and upscaling efforts in wastewater treatment systems based on calcium alginate liquid beads.

D. T. Tran, N.-K. Nguyen, A. S. Yadav, F. M. Galogahi, K. R. Sreejith, N.-T. Nguyen
Queensland Micro- and Nanotechnology Centre
Griffith University
170 Kessels Road, Nathan, Queensland 4111, Australia
E-mail: nam-trung.nguyen@griffith.edu.au

A. Chuang, M. Burford
Australian Rivers Institute
Griffith University
170 Kessels Road, Nathan, Queensland 4111, Australia

ⓘ The ORCID identification number(s) for the author(s) of this article can be found under https://doi.org/10.1002/aesr.202400112.

1. Introduction

The pervasive presence of algae, including harmful varieties, in bodies of water such as lakes, rivers, or oceans has been a major global environmental issue. The gradual accumulation of algal nutrients like nitrogen and phosphorus, termed eutrophication, stands as the primary cause of excessive algae growth.[1,2] Harmful algae, such as the dinoflagellate *Gymnodinium breve*, produce and release toxins into their surroundings, potentially inflicting detrimental health impacts on animals or humans upon direct contact with contaminated water. Furthermore, when the life cycle of algae concludes, their decomposition significantly depletes dissolved oxygen, potentially leading to the death of aquatic animals and consequent biodiversity decline.[3] To address this critical environmental challenge, a combination of direct control measures and preventative strategies has been employed. Direct methods encompass the use of flocculants to aggregate algae colonies or algicidal chemicals to impede their growth. Preventative measures focus on the regulation of nutrient levels in wastewater before its discharge into the environment. Recognized as proactive and environmental-friendly approaches, they can serve to mitigate the degree of algal blooms in water bodies of different sizes.[4,5]

The immobilization of nontoxic microalgae within calcium alginate hydrogel beads has been extensively investigated as a preventive measure for mitigating eutrophication. Over the years, numerous studies on using alginate hydrogel beads for nutrient removal from wastewater have been conducted, involving variations in microalgal species, alginate products, or bead geometries, contributing significantly to the advancement of wastewater treatment research.[6–9] The eco-friendly nature of sodium alginate, along with its straightforward synthesis processes and the ease of microalgae encapsulation, contributes significantly to the popularity of sodium alginate hydrogel beads. By consistently extruding sodium alginate aqueous droplets containing a specific quantity of microalgae into a calcium salt-based solution, numerous highly porous calcium alginate beads with a 3D structure can be produced. This process relies on the rapid ionotropic gelation between sodium alginate and calcium ions.

Subsequently, these beads are then immersed in targeted wastewater for an extended period to facilitate nutrient removal treatment. Microalgal cells encapsulated within the beads gradually absorb nutrient molecules from the surrounding wastewater through the transparent, permeable hydrogel, enabling their metabolism and reproduction. This process results in nutrient-depleted effluent, ready for the subsequent disinfection stage where any remaining microorganisms are eliminated by disinfectants. An additional advantage of alginate hydrogel beads is their capacity to maintain structural integrity even after prolonged immersion in wastewater, owing to the excellent stability of the hydrogel's 3D network. This allows the cell-laden hydrogel beads to be easily retrieved from the wastewater at the treatment's conclusion, offering possibilities for nutrient and microalgae recovery.

Calcium alginate liquid beads are well known for their distinctive core–shell structure, where the liquid core is entirely encased within a polymeric sodium alginate shell. Various methods have been employed to synthesize alginate liquid beads, such as droplet extrusion, microfluidic formation, and coacervation. These techniques enable the mass production of spherical, uniformly sized beads.[10–12] All these methods align with common principles: sodium alginate polymer strands envelop the aqueous or oil core, forming the alginate shell, subsequently crosslinked by calcium ions through ionotropic gelation. The process of generating calcium alginate liquid beads through single-nozzle droplet extrusion can also be referred to as the inverse gelation technique. This arises from the outward diffusion of calcium ions from the core droplets, where they crosslink with alginate polymer strands from the sodium alginate bath. Sodium alginate liquid beads can be engineered as carriers to encapsulate and deliver various cargos such as drugs, enzymes, and ointments.[13–15] Sodium alginate liquid beads can also be utilized for encapsulating and promoting the sustainable growth of cells, owing to the inherent unique features of hydrogel structures, including exceptional transparency and semipermeability. The efficacy of alginate liquid beads in culturing human cells has been substantiated by numerous researchers, solidifying the status of alginate liquid beads as a safe and reliable cell culture platform.[16–18]

Compared to the more prevalent hydrogel beads, liquid beads possess undeniable structural advantages. The encapsulation of microalgae inside the core of liquid beads can be characterized as a partial immobilization process. This is attributed to the fact that microalgal cells can still freely move, interact with growth factors, and reproduce in any direction confined within the alginate shell. This flexibility might benefit the overall growth process, leading to better growth efficiency and higher yields of microalgae. Simultaneously, while the crosslinked structure of hydrogel can promote adhesion and proliferation of immobilized cells, excessive crosslinking might impose spatial restrictions, limiting nutrient exchange and migration capabilities of the cells.[19–21] Consequently, microalgae immobilized in hydrogel beads might experience reduced growth rates and ultimately yield a lower biomass.

To the best of our knowledge, sodium alginate liquid beads have never been utilized for encapsulating and cultivating microalgae, despite the immense potential of this platform. In the present study, we investigated the potential application of sodium alginate liquid beads for microalgae encapsulation and their use in nutrient removal from wastewater. Employing a facile and convenient inverse gelation technique, we generated liquid beads and encapsulated microalgal cells. The treated effluent from upflow anaerobic sludge blanket (UASB) treatment served as the wastewater model to assess the immersed liquid beads. We prepared calcium alginate liquid beads with different calcium ion concentrations and examined their impact on bead morphology, cell growth, nutrient removal efficiency, and stability through characterization techniques such as scanning electron microscopy (SEM) imaging, cell counting, discrete chemical analysis, geometrical measurements, and mechanical compression.

2. Experimental Section

2.1. Materials and Apparatus

Sodium alginate, calcium lactate, and carboxymethyl cellulose (CMC) were acquired from Sigma–Aldrich. The *Chlorella vulgaris* microalgal strain, codename CS-41, was obtained from the Commonwealth Scientific and Industrial Research Organisation. The BG-11 culture medium was collected from the Australian Rivers Institute at Griffith University, Australia. The effluent generated from the UASB digestion process was supplied by Urban Utilities as a real wastewater sample. Prior to the nutrient removal treatment experiment, the UASB effluent was decanted to eliminate residual solid particles and then sterilized using a 0.22 μm filter membrane to remove any potentially present bacteria.

2.2. Preculture of Microalgae

C. vulgaris was subcultured in sterilized BG-11 medium in an enclosed cultivation chamber at 25 °C under LED growth light with 12:12 h light–dark cycle. After 6 days, microalgal cells were separated from the growth medium at exponential growth phase using centrifugation (4500 rpm, 15 min), and then resuspended into Milli-Q water. This procedure was used to prepare three microalgal stocks for the encapsulation of cells in liquid beads, followed by nutrient removal of beads in UASB effluent.

2.3. Encapsulation of Microalgae Inside Liquid Beads and UASB Effluent Treatment Experiment

The calcium alginate liquid beads with core–shell structure were produced using inverse gelation technique.[22,23] In this research, we thoroughly examined various calcium-based salts to serve as the source of calcium ions for ionic crosslinking of sodium alginate. The release of residual anions from the liquid beads could potentially affect the surrounding aquatic environment upon the discharge of treated effluent. We made the decision not to utilize calcium chloride, despite its widespread use, due to the potential toxicity of chloride ions to certain aquatic species.[24–26] Instead, we opted for calcium lactate, a substance that has been demonstrated to be nontoxic upon oral consumption by both humans and animals.[27] Selecting calcium lactate ensures the nontoxicity and biocompatibility of the liquid beads for potential applications in recovery and repurposing. **Figure 1** illustrates the systematic
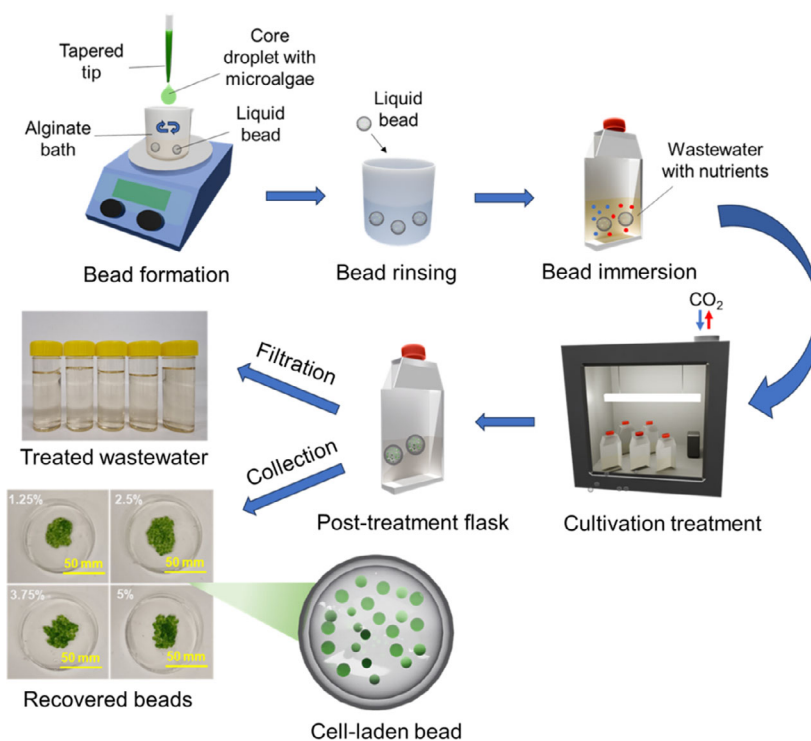
Figure 1. Schematic depicting the generation of calcium alginate liquid bead-microalgae systems and their application in wastewater treatment.

formation of liquid bead-microalgae systems and their utilization in wastewater treatment. First, the core solution of liquid beads was prepared by adding CMC (1% w/v) powder and calcium lactate into Milli-Q water under vigorous stirring (800 rpm). To investigate the effect of calcium ion concentrations on the characteristics of liquid beads containing microalgal cells, four core solutions were prepared with different concentrations (1.25%, 2.5%, 3.75%, and 5% w/v) of calcium lactate. It is worth noting that 5% represents the solubility of calcium lactate in water. Then, *C. vulgaris* microalgal stock was added into each of the core solutions under moderate stirring (500 rpm). The volume-to-volume ratio between the stock culture and the core solution was fixed at 1:10. The initial concentration of microalgae in the core solution was 1.24×10^6 cells mL^{-1}. For high-throughput liquid bead generation, we established a system comprising a syringe pump, PTFE tubing, a magnetic stirrer, a tapered tip, and dedicated software (SPM100 Syringe Pumps Control) for precise flow rate control. The core solution-microalgae stock mixture was extruded out of the system with a flow rate of 1 mL min^{-1} into a sodium alginate bath (1% w/v) under slow stirring speed, resulted in the formation of liquid beads. Subsequently, approximately 100 beads were collected, thoroughly rinsed with water to get rid of excess calcium ions, and then introduced into culture flasks containing sterilized 30 mL of UASB effluent for nutrient removal treatment experiment. The liquid beads generated from core solution with 1.25%, 2.5%, 3.75%, and 5% concentration of calcium lactate are labeled a Ca125, Ca250, Ca375, and Ca500 for convenient discussion of results analysis.

During the treatment period, the culture flasks containing UASB effluent and liquid beads and flasks with only UASB effluent as control samples were placed in an enclosed treatment chamber with controlled temperature and lighting. The temperature and lighting regime were like the preculture process. The photosynthetic photon flux density of the LED growth light in this study was set at 57 µmol m^{-2} s^{-1}. The total treatment of beads in UASB effluent was 13 days to ensure effective removal of nutrients. Following the treatment, both treated UASB effluent and liquid beads were collected and stored under proper conditions for further characterizations. The treated effluent was sterile filtered using 0.45 µm filter to get rid of possible residual bacteria and stored under freezing conditions ($-18\,°C$), whereas the dried beads were collected and stored at 4 °C. We also performed three independently repeated batches of nutrient removal experiments where the liquid bead-microalgae systems were fabricated from three different microalgal stocks to ensure the reliability of final treatment results.

2.4. Characterizations

2.4.1. Geometries

The geometries of calcium alginate liquid beads, including the volume, bead diameter, core diameter, and shell thicknesses, were measured by analyzing the digital images of liquid beads captured before and after treatment. Image analysis was conducted using ImageJ software (NIH, USA). The images were captured using a 1.3 MP Ximea Color CMOS Camera with USB 3.1 interface, supported by a VZM 450 Zoom Imaging Lens (Edmund Optics).

**ADVANCED
SCIENCE NEWS**

www.advancedsciencenews.com

**ADVANCED
ENERGY & SUSTAINABILITY
RESEARCH**

www.advenergysustres.com

Sphericity factor calculation was adopted to determine the sphericity of the beads. The equation for the sphericity factor is[23–29]

$$s = \frac{d_{\max} - d_{\min}}{d_{\max} + d_{\min}} \qquad (1)$$

where S is the sphericity factor, $d_{\max}$ is the maximum diameter, and $d_{\min}$ is the minimum diameter of the beads.

2.4.2. Morphologies

The morphologies of calcium alginate liquid beads were examined using SEM imaging before and after treatment. Initially, the liquid beads underwent freeze-drying to eliminate the aqueous core, followed by a gold sputtering process to enhance the shell's conductivity. The surface and porosities of the shell were observed using the JEOL JSM-6510LV low-vacuum scanning electron microscope.

2.4.3. Compression Strength

Compression behavior of liquid beads before and after treatment were investigated using a parallel-plate compression setup, which was used in our previous study.[30] The setup comprises a moveable top plate and a precision balance as the stationary bottom plate. The vertical movement of the top plate is controlled by a translation stage, and the compression force is recorded using a balance. Compression profile of the beads was visualized by plotting the force–displacement curve using the recorded compression data.

2.4.4. Cell Growth Pattern

Growth behavior of microalgal cells encapsulated inside the liquid beads during the treatment period was determined by analyzing cell growth profiles and specific growth rate of the cells.

To generate cell growth profiles, we determine daily cell number by using cell counting technique. Every day, a total of three beads (one from each experimental batch) were extracted from the culture flasks for the cell counting process. Initially, calcium alginate liquid bead was obtained from the culture flask and immersed in a specific volume of 0.2 M sodium citrate solution. The mixture was vigorously stirred using a vortex mixer for 2 min to ensure complete dissolution of the alginate shell. Subsequently, the resulting solution (10 μL) was withdrawn and introduced into the Neubauer cell counting chamber. This chamber was then positioned beneath a Nikon Eclipse Ti2 Inverted Microscope for cell observation. Images of the cells were captured using the microscope. The acquired photos were then analyzed with ImageJ (NIH, USA) to precisely count the cells and to determine the final cell numbers. The equation used to compute cell number for liquid beads were derived as follows

$$P = \frac{N \times D}{V_c} \qquad (2)$$

where P is the final cell number (cells mL^{-1}), N is the average cell number counted in one 1 mm^2 counting square, V_c is the volume

of the counting square ($V_c = 0.1$ μL), and D is the dilution factor. The dilution factor for liquid beads is $D = (400 + V_{\text{bead}})/V_{\text{core}}$, where V_{bead} (μL) is the total volume of the bead and V_{core} (μL) is the volume of the core.

The specific growth rate is a constant indicating the cell number increase per unit time during exponential growth stage, which relies on the accurate determination of the cell growth profile. Initially, cell number data over time were plotted in a semi-log curve with the y-axis on a natural logarithmic scale. The exponential growth phase was then identified by pinpointing the period where cell number data formed a straight line with a positive slope on the semilog curve. Subsequently, the specific growth rate was computed based on the slope of this straight line.

$$\mu = \frac{dP}{dt} \qquad (3)$$

where μ is the specific growth rate (day^{-1}) and dP/dt is the rate of increase of cell number.

2.4.5. Nutrient Removal Efficiency

Nutrient removal efficiency of suspended calcium alginate liquid beads in UASB effluents was investigated by measuring the concentrations of ammonium (NH_4^+) and dissolved phosphate (PO_4^{3-}) in effluents. This measurement was conducted before and after treatment using a fully automated Thermo Scientific Gallery Plus Discrete Analyzer.

2.4.6. Statistical Analysis

The statistical analysis of the geometries of liquid beads was carried out using SPSS Statistics version 29.0.0 (IBM, USA). Analysis of variance and Tukey's test were chosen as the statistical models to verify the statistically significant differences ($p < 0.05$) among the geometric parameters of liquid beads with different calcium ion concentrations.

3. Results and Discussions

3.1. Morphologies of Liquid Beads

Morphologies of the liquid bead shells generated with different calcium ion concentrations were examined through SEM images. A crucial step in sample preparation involved utilizing the freeze-drying rather than ambient drying to minimize shrinkage of the porous structure of the liquid bead shells during SEM measurement. Despite this effort, SEM images revealed the postdrying collapse of the pore networks occurred in beads collected after treatment experiments, resulting in a thin film structure without observable pores. This collapse indicated weakened mechanical properties of the liquid beads, an aspect that will be further investigated in subsequent sections. **Figure 2** illustrates the morphologies of the liquid bead shells before the treatment. Notably, the image of the Ca125 bead (Figure 2a) showed hardly discernible pores, suggesting shell collapse possibly due to poor resistance of the shell against the sublimation of ice molecules during freeze-drying. In contrast, Ca250, Ca375, and Ca500 beads maintained postdrying porous structures with varying
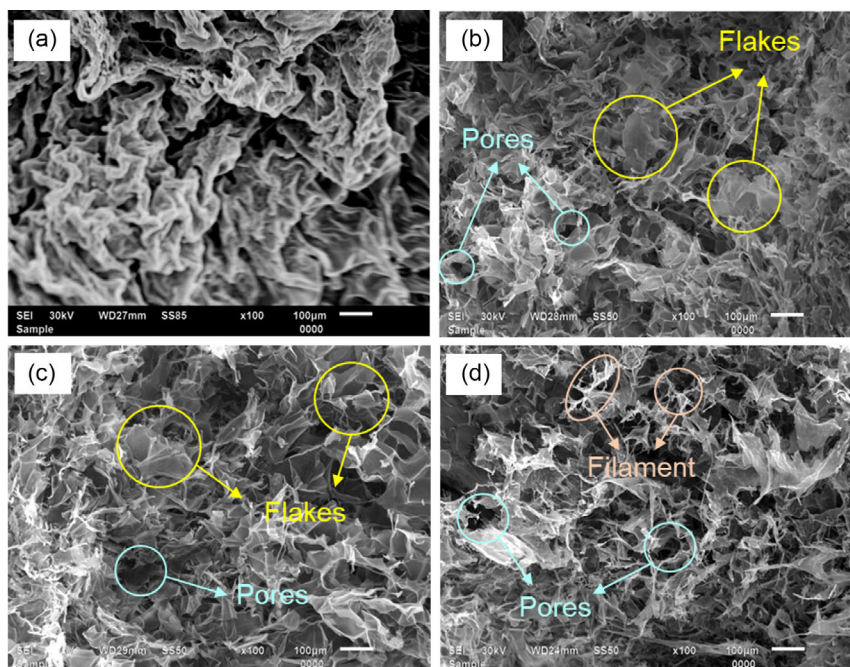
**ADVANCED
SCIENCE NEWS**

www.advancedsciencenews.com

**ADVANCED
ENERGY & SUSTAINABILITY
RESEARCH**

www.advenergysustres.com

Figure 2. SEM images of the shell of calcium alginate liquid beads generated with different calcium ion concentrations: a) Ca125, b) C250, c) Ca375, and d) Ca500. Scale bars are 100 μm.

morphologies. SEM images of Ca250 and Ca375 shells (Figure 2b,c) revealed alginate polymer strands adhering and forming flakes, resulting in an incomplete crosslinked structure with limited pore presence. Conversely, the Ca500 shell displayed clearer boundaries between pores, with pore walls primarily composed of filament-like alginate strands rather than flakes. The introduction of higher amounts of calcium lactate led to increased crosslinking between calcium ions and alginate polymer strands, generating more crosslinking nodes and forming a more intricate 3D network structure.

3.2. Microalgal Cell Growth Behavior

Generally, numerous types of microorganisms including bacteria, fungi, protozoa, and algae coexist in nontreated wastewater. The abundance of essential nutrients like nitrogen and phosphorus, in both soluble inorganic and organic compounds, provides an optimal environment for metabolic activities, rapid growth, and reproduction of these microorganisms.[31] In this study, we aimed to absorb nitrogen and phosphorus using liquid beads encapsulating microalgae by prolonged submergence in UASB effluent.

Despite pretreatment of UASB effluent, such as decanting and sterile filtration, it is still necessary to perform daily growth analysis of microalgae. This ensures that the healthy growth of microalgae is the sole contributor to the removal of nitrogen and phosphorus from UASB effluent. To study growth behavior of microalgae *C. vulgaris* inside liquid beads during the treatment process, we analyzed the microscopic photos of the cells suspended in cell counting chamber and calculated the cell number using Equation (2). All the platforms in the same batch had the

same starting cell number (1.24×10^6 cells mL^{-1} on average). The microscopic photos of extracted cells in **Figure 3**a depicted similar cell sizes across all beads, with Ca500 beads showing a higher cell count at the experiment's conclusion.

For a comprehensive understanding of cell growth behavior, daily average cell numbers were consolidated to generate final cell number curves (Figure 3b). Overall, these curves illustrate that the growth of encapsulated microalgae in UASB effluent followed typical three-phase growth patterns observed during microalgae culturing in growth media. These phases include lag phase, exponential growth phase, and stationary phase.[32,33] Microalgae within Ca500 beads displayed the steepest slope of exponential growth compared to other beads, reaching the stationary phase by the end of the experiment. Meanwhile, microalgae in other beads likely remained in the exponential growth phase. To further verify the growth rate of microalgae in the beads, we also extracted the cell numbers at exponential growth phase for each type of liquid beads to calculate the specific growth rate using Equation (3).

The calculated specific growth rates (Figure 3c) indicate that Ca500 exhibited the highest growth rate, consistent with its highest gradient in exponential growth phase. The rapid growth of microalgae in Ca500 beads likely depleted nutrients faster, leading to progression into the stationary phase by the end of the treatment. Additionally, the rapid growth in Ca500 beads resulted in the highest maximum cell number (8.05×10^7 cells mL^{-1}), followed by Ca375, Ca250, and Ca125 beads (5.2×10^7, 3.85×10^7, and 2.72×10^7 cells mL^{-1}, respectively). Consequently, the Ca500 beads demonstrated the best cell growth performance with the fastest growth and the least time needed to achieve the maximum cell number. The impressive
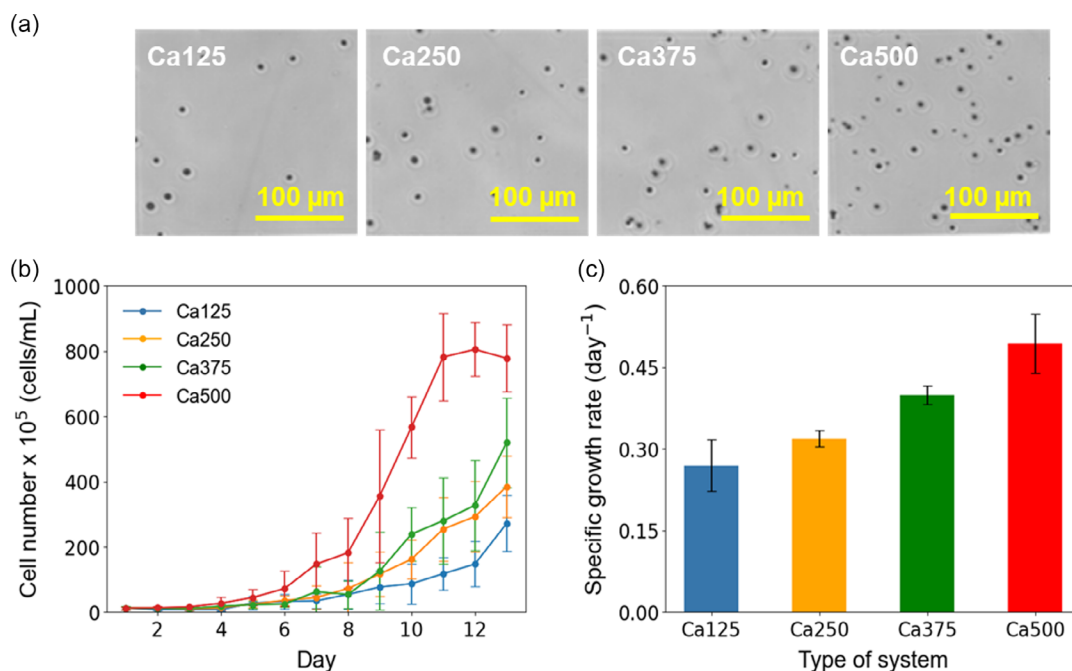
Figure 3. Growth behavior of microalgal cells in calcium alginate liquid beads generated with different calcium ion concentrations: a) cell number profile and derived specific growth rate of microalgal cells inside liquid beads; b) microscopic images of microalgal cells at day 13; and c) specific growth rates of microalgal cells inside liquid beads. The error bars represent the standard deviation of three measurements.

cell growth of Ca500 beads is linked to its ability to preserve the crosslinked network structure under the impact of a process called osmotic swelling. This phenomenon usually occurs between two regions with different solute concentrations that are separated by a semipermeable membrane. Water migrates from aqueous region with lower concentration of solutes (UASB effluent) into aqueous region with higher concentration of solutes (core of the beads), leading to the expansion of the core volume.[34,35] The shell of Ca125, Ca250, and Ca375 beads with lower degree of crosslinking might suffer from the stress arising from core expansion, resulted in the densely packed structure with reduction in porosities overtime.[36] Lower porosities of alginate shell might be associated with poorer diffusion of nutrients and carbon dioxide, leading to less effective cell growth.

3.3. Nutrient Removal Efficiency

Ammonium (NH_4^+) and phosphate ions (PO_4^{3-}) are two major inorganic nutrients that are inadvertently introduced into wastewater by a wide range of municipal, industrial, and agricultural activities. Ammonium is the most preferable source of nitrogen for many algae and microorganism species, particularly the fast-growing ones. This is attributed to its less energy-intensive assimilation process into cellular compartments, thereby benefitting the metabolism and growth of microalgal cells.[37,38] Meanwhile, phosphate ion is the primary inorganic phosphorus present in wastewater, readily incorporating into the cell bodies for metabolism process.[39,40] If untreated wastewater containing both ammonium and phosphate is discharged into water bodies, the environmental consequences from eutrophication could be

catastrophic. Thus, tertiary nutrient removal treatment of wastewater is essential to effectively reduce ammonium and phosphate concentrations, minimizing the risk of eutrophication upon effluent discharge into the environment.

Here, we explore nutrient removal from wastewater utilizing liquid beads generated above to determine and compare nutrient removal efficiencies. We measured the concentrations of ammonium and phosphate ions in the sterile filtered UASB effluents before and after nutrient removal treatment (**Figure 4**). The liquid bead-microalgae systems effectively removed both ammonium and phosphate from UASB effluents simultaneously. The results indicated diverse removal efficiencies among the different systems. The crosslinking degree of the alginate shell significantly influenced nutrient assimilation behaviors. In general, we observed a higher nutrient uptake in liquid beads containing a greater concentration of calcium ions in the shell. The Ca500 bead-microalgae system displayed the lowest concentrations of both ammonium and phosphate, resulting in remarkable removal efficiencies for these nutrients (up to 67.3% and 72.6%, respectively). Statistical analysis confirmed the superior effectiveness of Ca500 beads in removing ammonium compared to other liquid beads. Meanwhile, the significance of phosphate removal efficiency between Ca500 and Ca375 beads was not statistically established. Nonetheless, the statistical analysis of post-treatment phosphate concentration underscored the direct proportionality between phosphate removal efficiency and the concentration of calcium ions in liquid beads, suggesting that higher concentrations of calcium ions correlate with improved phosphate removal efficiency.

As discussed in the previous section on cell growth analysis, Ca500 beads demonstrated superior porosity preservation during
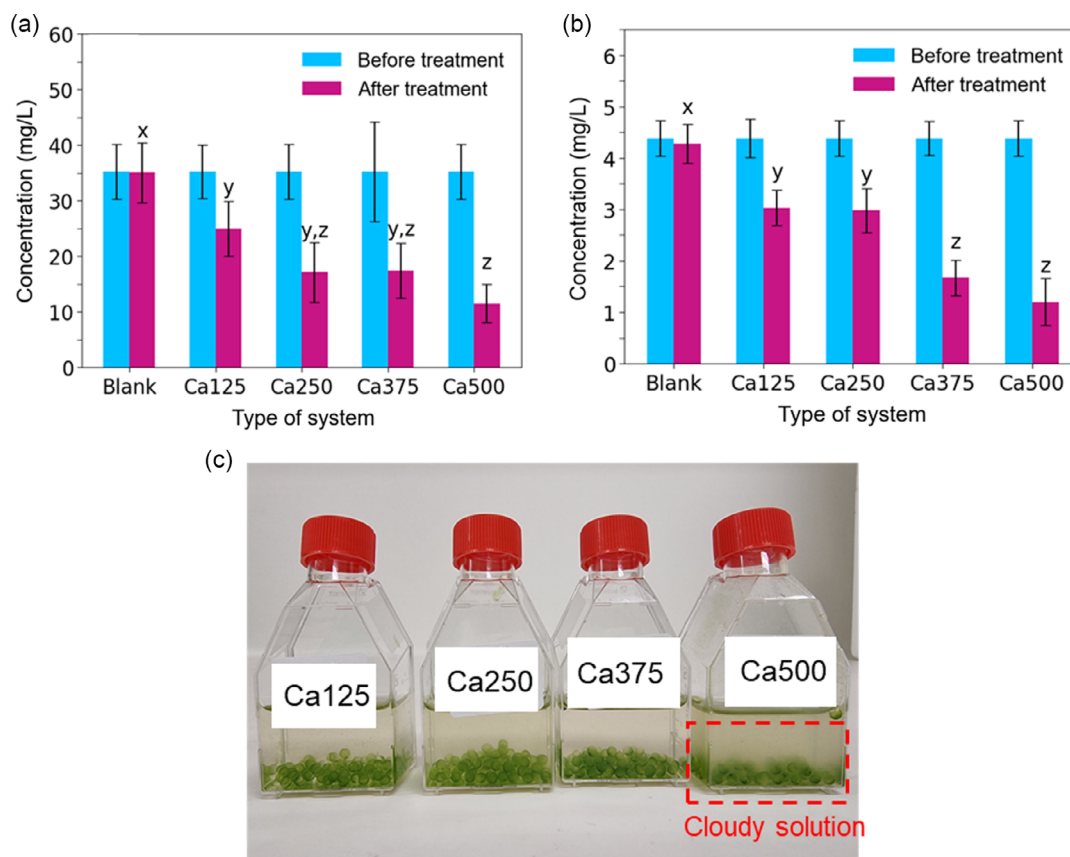
**ADVANCED
SCIENCE NEWS**

www.advancedsciencenews.com

**ADVANCED
ENERGY & SUSTAINABILITY
RESEARCH**
Open Access

www.advenergysustres.com

Figure 4. Nutrient removal behaviors of liquid bead-microalgae systems: a) concentrations of ammonium ions before and after treatment; b) concentrations of phosphate ions before and after treatment; and c) culture flasks at the final day of treatment. The error bars represent the standard deviation of three measurements. Different annotated letters represent statistically significant differences ($P < 0.05$), with "x", "y", and "z" corresponding to data after treatment.

the entire immersion period compared to other liquid beads, likely facilitating nutrient diffusion and higher microalgal nutrient uptake. Additionally, phosphate removal by Ca500 beads may involve an abiotic process known as phosphorus precipitation.[41] Residual calcium ions and possibly leaked calcium ions from alginate shell might react with some phosphate ions in UASB effluent to form calcium phosphate salt particles, which precipitates out of the solution.[42,43] The release of calcium ions may occur via an ion exchange process between the calcium ions within the liquid beads and trace amounts of monovalent ions present in the UASB effluent.[44,45] As shown in the image of culture flasks at the final day of treatment (Figure 4c), this phenomenon was observed only in the effluent containing Ca500 beads, with the cloudy appearance indicating the presence of precipitates. The precipitates were removed during the sterile filtration process, contributing to the ultimate reduction of phosphate ions in the effluent treated by Ca500 bead-microalgae system.

3.4. Stabilities of Liquid Beads in UASB Effluent

Structural degradation or mechanical breakdown in harsh aqueous media such as wastewater is common phenomenon associated with polymeric beads. This is attributed to the possible

interferences of ions present in wastewater with the polymer backbone of the beads. Poor mechanical and structural integrity of beads might lead to leakage of microalgal cells into the wastewater. Additionally, an intensive post-treatment separation process might be required to remove the leaked cells out of the contaminated effluent.[39] In this study, we further investigated the mechanical stabilities and structural stabilities of liquid beads by measuring geometries and characterization of compression behavior of liquid beads before and after treatment experiment.

3.4.1. Structural Stabilities

We collected a total of 40 beads for each calcium concentration before and after wastewater treatment experiment (20 beads before the wastewater treatment and 20 beads after the treatment) to investigate the structural stabilities of alginate liquid beads. High-quality images of each bead were captured and precisely analyzed using ImageJ (NIH, USA).

Figure 5 shows the digital images of beads. It is obvious all the liquid beads possessed good shell transparency and highly spherical shapes. The more blurred image of Ca125 bead before treatment with less reflection of lighting indicated its superior transparency over other beads. This is most likely due to the less
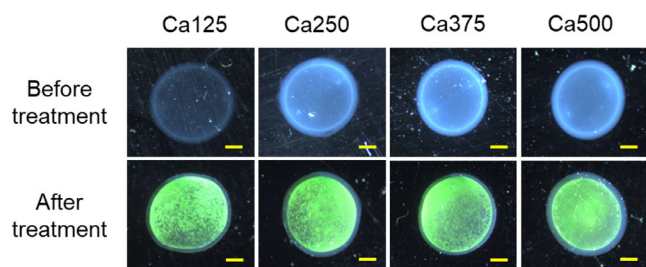
2400112 (7 of 11)

**ADVANCED
SCIENCE NEWS**

www.advancedsciencenews.com

**ADVANCED
ENERGY & SUSTAINABILITY
RESEARCH**
Open Access

www.advenergysustres.com

Figure 5. Digital images of calcium alginate liquid beads generated with different calcium ion concentrations before and after treatment of UASB effluent. Scale bars are 1 mm.

crosslinking structure of the shell, allowing more light to pass through. After treatment, microalgal cells could be seen in the cores, and also there were visible reduction in shell thicknesses. The detailed analysis shown in **Figure 6** provided further insights into the changes of the geometries of beads before and after treatment. It is obvious that all the beads had the similar diameter (≈4.3 mm) and slight differences between their core diameters before and after treatment. The differences are more obvious

for the shell thicknesses, where Ca500 beads had the thickest shells, followed by Ca250, Ca375, and Ca125. Alginate liquid beads produced by inverse gelation are known for their layer-by-layer alginate assembly principle. Core solution droplet with higher calcium ion concentration likely adopted this mechanism better by attracting more alginate molecules and formed the shell with more alginate layers, resulted in thicker shells.[46] The multilayer shell formation seemed to also enhance the structural morphology of the beads. Both Ca375 and Ca500 beads maintained a highly spherical structure before and after treatment, with a sphericity value below 0.05.

Figure 6 indicates the effect of bead prolonged immersion in UASB effluent on the overall bead diameter, core diameter, and the shell thicknesses. While both bead diameter and core diameter of all the beads increased moderately after the treatment, the shell thickness reduced. These results are in good agreement with the digital images. The increases in bead diameter, core diameter, and simultaneous reduction in shell thicknesses can be attributed to the osmotic swelling process discussed in the previous section. However, thanks to the elasticity features of alginate hydrogel, no bursting or major degradation of the shell was observed for all the beads, and microalgae cells still
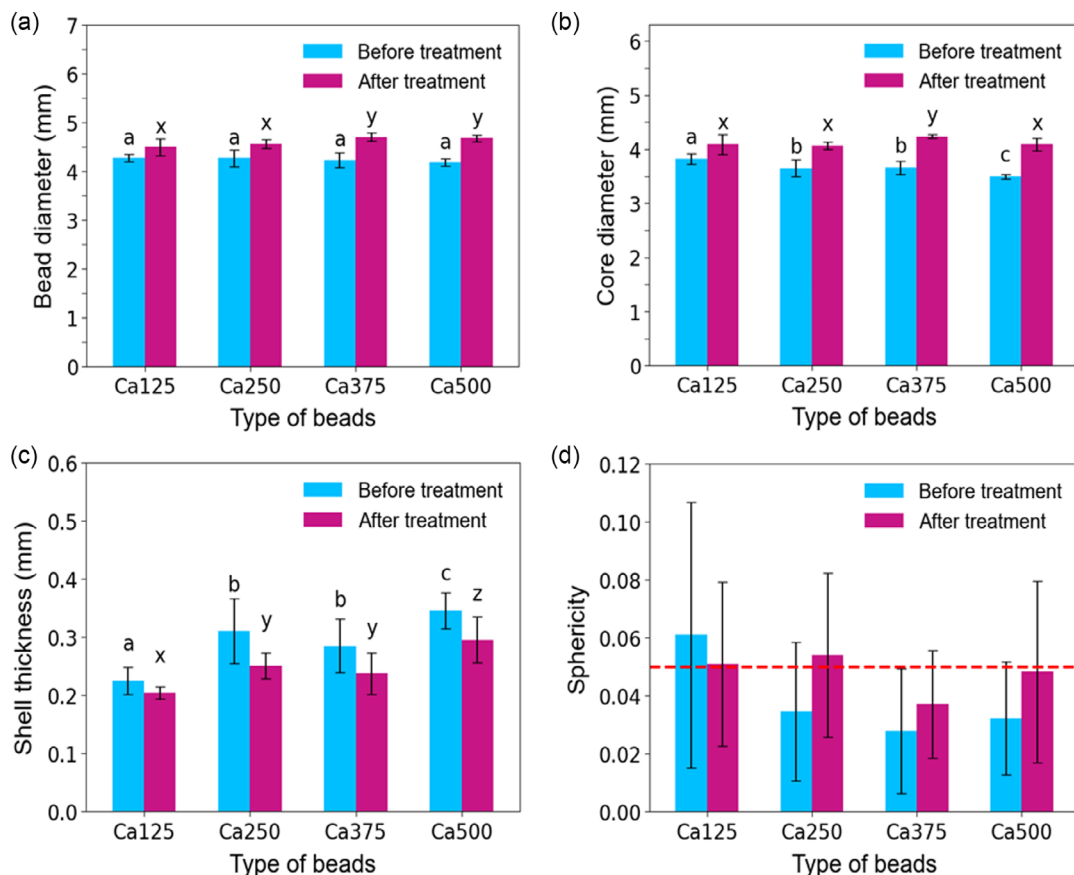

Figure 6. Effect of calcium ion concentrations on different geometrical parameters of calcium alginate liquid beads before and after treatment of UASB effluent: a) bead diameter; b) core diameter; c) shell thickness; and d) sphericity. The error bars represent the standard deviation of three measurements. Different annotated letters represent statistically significant differences ($P < 0.05$), with "a", "b", "c" corresponding to data before treatment and "x", "y", "z" corresponding to data after treatment.

remained intact within the core of the beads after 13 days of treatment.

3.4.2. Mechanical Stabilities

In this study, we chose parallel compression plate as the standard method to investigate and compare the mechanical stabilities of alginate liquid beads. Compression test using parallel plate is a widely recognized mechanical test for studying mechanical properties of spherical solid objects due to its versatility, time efficiency, and highly consistent testing methodologies.[47–49] Moreover, this test offers valuable insights into how the liquid beads respond to stresses in real-world situations, for example, when the beads are tightly stacked prior to dispensing into wastewater pond for treatment, or during the final bead collection process when the mixture of beads and treated wastewater is required to pass through a mesh filter.

Prior to compression test, we collected totally ten beads for each calcium ion concentration before and after wastewater treatment experiment (five beads before treatment and five beads after treatment). Each bead was placed on the balance and subjected to compression of the upper plate with consistent displacement intervals. **Figure 7** displays the typical force–displacement curves of each bead before and after treatment. From these curves, we can see that Ca500 beads exhibited superior compression performance both before and after wastewater treatment. Meanwhile, before the treatment, Ca125 beads with lowest amount of calcium ion collapsed earlier than other beads (at 2.25 mm displacement), indicating its scarcely crosslinked structure with poor resistance to compression. It can also be seen from Figure 7a,b that the prolonged immersion of liquid beads in UASB effluent had substantial impact on their compression performance. All the beads experienced mechanical breakdown at a relatively small displacement (1.75 mm), and the final compressive forces before failure of all the beads after treatment experienced an approximate fivefold decrease. The reduction in shell thicknesses, the intrusion of water into the shell, coupled with possible leakage of calcium ions from the shell are most likely the causes for the decline in the resistance to plastic deformation of beads.[50]

4. Conclusions

In this study, we successfully encapsulated microalgae *C. vulgaris* inside the core of calcium alginate liquid beads and leveraged the nutrient assimilation mechanism of microalgae for removing nutrients from wastewater. All liquid beads crosslinked with varying calcium ion concentrations were easily collected without experiencing degradation or structural breakdown at the end of the nutrient removal experiment. Our findings suggest that the quantity of calcium ions presenting in the core droplets prior to gelation significantly influenced the performance of liquid beads in all aspects. Specifically, morphological characterization based on SEM measurement revealed that Ca500 beads exhibit the most comprehensive 3D network structure, signifying efficient crosslinking between alginate and higher quantity of calcium ions. Cell growth investigation demonstrated that Ca500 beads achieve the highest cell count and growth rate, likely due to their ability to maintain crosslinked structures during the treatment period. This aligns with nutrient removal efficiencies, as microalgae in Ca500 beads achieve removal rates of up to 67.3% for ammonium and 72.6% for phosphate. Regarding structural stability, Ca500 and Ca375 beads maintained their spherical shapes well after the treatment (sphericities < 0.05). For mechanical stability, declines in compression performance after the wastewater treatment can be observed for all the beads, according to the force–displacement curves. In addition, the compression resistance was proportional to the quantity of calcium ions in the beads, with Ca500 beads as the top performer. The intriguing results of this study provide a foundation for further advancements in optimizing the fabrication of calcium alginate liquid bead-microalgae systems for wastewater treatment. Exploring the utilization of large-scale bioreactors integrated with advanced cell culture techniques to enhance cell growth and optimize nutrient removal efficiency could be a promising avenue for the next stage of research. Additionally, future studies could explore the recovery of post-treatment cell-laden liquid beads, offering opportunities for repurposing. These repurposed beads hold potential applications in various fields, including the production of biofertilizers and biostimulants.[51,52]
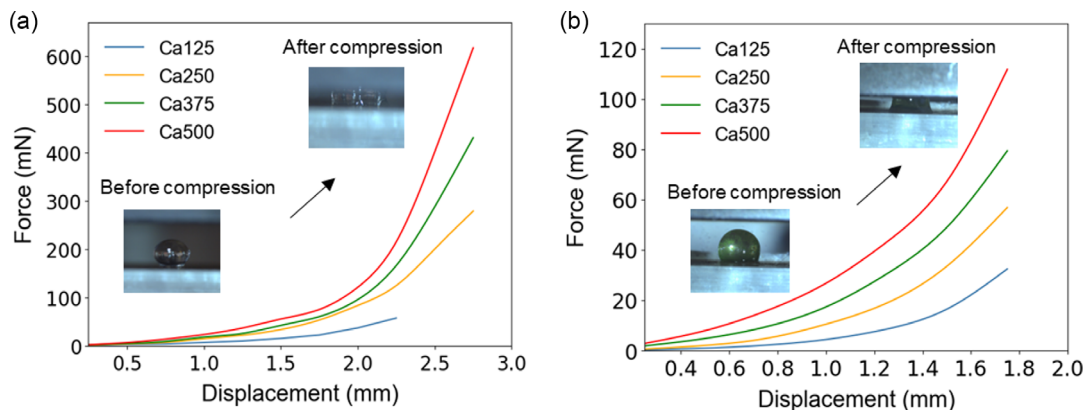

Figure 7. Effect of calcium ion concentrations on compression behaviors of calcium alginate liquid beads: a) force–displacement curves of liquid beads before treatment of UASB effluent and b) force–displacement curves of liquid beads after treatment of UASB effluent.

Conflict of Interest

The authors declare no conflict of interest.

Data Availability Statement

The data that support the findings of this study are available from the corresponding author upon reasonable request.

[1] L. Zhu, W. Shi, B. Van Dam, L. Kong, J. Yu, B. Qin, *Environ. Sci. Technol.* **2020**, *54*, 6194.

[2] M. Preisner, E. Neverova-Dziopak, Z. Kowalewski, *Ambio* **2021**, *50*, 413.

[3] B. Balaji-Prasath, Y. Wang, Y. P. Su, D. P. Hamilton, H. Lin, L. Zheng, Y. Zhang, *Environ. Chem. Lett.* **2022**, *20*, 3133.

[4] K. J. Erratt, I. F. Creed, C. G. Trick, *Harmful Algae* **2022**, *116*, 102264.

[5] E. Zohdi, M. Abbaspour, *Int. J. Environ. Sci. Technol.* **2019**, *16*, 1789.

[6] A. Saxena, B. Mishra, A. Tiwari, *Environ. Technol. Innovation* **2021**, *23*, 101736.

[7] K. Limrujiwat, S. Suphan, K. Sujarit, T. Lomthong, W. Khetkorn, *Biocatal. Agric. Biotechnol.* **2022**, *43*, 102419.

[8] M. Han, C. Zhang, S. H. Ho, *Environ. Sci. Ecotechnol.* **2023**, *14*, 100227.

[9] S. F. Mohsenpour, S. Hennige, N. Willoughby, A. Adeloye, T. Gutierrez, *Sci. Total Environ.* **2021**, *752*, 142168.

[10] E. Martins, D. Renard, Z. Adiwijaya, E. Karaoglan, D. Poncelet, *J. Microencapsulation* **2017**, *34*, 82.

[11] L. P. H. Bastos, B. de Sa Costa, R. P. Siqueira, E. E. Garcia-Rojas, *Int. J. Biol. Macromol.* **2020**, *160*, 861.

[12] L. Yu, Q. Sun, Y. Hui, A. Seth, N. Petrovsky, C. X. Zhao, *J. Colloid Interface Sci.* **2019**, *539*, 497.

[13] S. Petraitytė, A. Šipailienė, *LWT Food Sci. Technol.* **2019**, *110*, 307.

[14] D. T. Tran, A. S. Yadav, N. K. Nguyen, P. Singha, C. H. Ooi, N. T. Nguyen, *Small* **2023**, *2303435*. https://doi.org/10.1002/smll.202303435

[15] O. Gryshkov, V. Mutsenko, D. Tarusin, D. Khayyat, O. Naujok, E. Riabchenko, Y. Nemirovska, A. Danilov, A. Y. Petrenko, B. Glasmacher, *Int. J. Mol. Sci.* **2021**, *22*, 3096.

[16] W. Bouhlel, J. Kui, J. Bibette, N. Bremond, *ACS Biomater. Sci. Eng.* **2022**, *8*, 2700.

[17] N. Landazuri, R. D. Levit, G. Joseph, J. M. Ortega-Legaspi, C. A. Flores, D. Weiss, A. Sambanis, C. J. Weber, S. A. Safley, W. R. Taylor, *J. Tissue Eng. Regener. Med.* **2016**, *10*, 222.

[18] S. Nebel, M. Lux, S. Kuth, F. Bider, W. Dietrich, D. Egger, A. R. Boccaccini, C. Kasper, *Bioengineering* **2022**, *9*, 66.

[19] Y. Fu, X. Xie, Y. Wang, J. Liu, Z. Zheng, D. L. Kaplan, X. Wang, *ACS Biomater. Sci. Eng.* **2021**, *7*, 2734.

[20] T. Kopač, Ž. Boček, K. P. van Midden, M. Klemenčič, A. Ručigaj, *Biochem. Eng. J.* **2023**, *199*, 109070.

[21] M. Al-Mossawi, H. Warren, P. J. Molino, P. Calvert, M. in het Panhuis, *Mater. Adv.* **2021**, *2*, 1369.

[22] J. Tan, Y. Luo, Y. Guo, Y. Zhou, X. Liao, D. Li, X. Lai, Y. Liu, *Int. J. Biol. Macromol.* **2023**, *239*, 124275.

[23] J. Zhao, Q. Guo, W. Huang, T. Zhang, J. Wang, Y. Zhang, L. Huang, Y. Tang, *Polymers* **2020**, *12*, 688.

[24] N. Wang, C. D. Ivey, R. A. Dorman, C. G. Ingersoll, J. Steevens, E. J. Hammer, C. R. Bauer, D. R. Mount, *Environ. Toxicol. Chem.* **2018**, *37*, 3041.

[25] J. R. Elphick, K. D. Bergh, H. C. Bailey, *Environ. Toxicol. Chem.* **2011**, *30*, 239.

[26] M. A. Rogalski, E. S. Baker, C. M. Benadon, C. Tatgenhorst, B. R. Nichols, *Evol. Appl.* **2024**, *17*, e13668.

[27] E. P. o. Additives, F. Products or Substances used in Animal, V. Bampidis, G. Azimonti, M. L. Bastos, H. Christensen, B. Dusemund, M. Kouba, M. Kos Durjava, M. Lopez-Alonso, S. Lopez Puente, F. Marcon, B. Mayo, A. Pechova, M. Petkova, F. Ramos, Y. Sanz, R. E. Villa, R. Woutersen, G. Aquilina, G. Bories, J. Gropp, C. Nebbia, M. L. Innocenti, *EFSA J.* **2019**, *17*, e05914.

[28] B. Balanc, A. Kalusevic, I. Drvenica, M. T. Coelho, V. Djordjevic, V. D. Alves, I. Sousa, M. Moldao-Martins, V. Rakic, V. Nedovic, B. Bugarski, *J. Food Sci.* **2016**, *81*, E65.

[29] E. S. Chan, B. B. Lee, P. Ravindra, D. Poncelet, *J. Colloid Interface Sci.* **2009**, *338*, 63.

[30] F. M. Galogahi, H. An, Y. Zhu, N.-T. Nguyen, *J. Mol. Liq.* **2021**, *344*, 117726.

[31] M. A. Yaakob, R. Mohamed, A. Al-Gheethi, R. Aswathnarayana Gokare, R. R. Ambati, *Cells* **2021**, *10*, 393.

[32] N.-K. Nguyen, A. Chuang, P. Singha, G. Kijanka, M. Burford, C. H. Ooi, N.-T. Nguyen, *React. Chem. Eng.* **2023**, *8*, 2710.

[33] J. F. L. Duval, A. Razafitianamaharavo, I. Bihannic, M. Offroy, N. Lesniewska, B. Sohm, H. Le Cordier, C. Mustin, C. Pagnout, A. Beaussart, *Algal Res.* **2023**, *69*, 102955.

[34] J. Guo, L. Hou, J. Hou, J. Yu, Q. Hu, *Micromachines* **2020**, *11*, 444.

[35] W. Zhang, A. Abbaspourrad, D. Chen, E. Campbell, H. Zhao, Y. Li, Q. Li, D. A. Weitz, *Adv. Funct. Mater.* **2017**, *27*, 1700975.

[36] Y. Shi, D. Xiong, Y. Liu, N. Wang, X. Zhao, *Mater. Sci. Eng., C* **2016**, *65*, 172.

[37] G. Salbitani, S. Carfagna, *Sustainability* **2021**, *13*, 956.

[38] X. Liu, K. Ying, G. Chen, C. Zhou, W. Zhang, X. Zhang, Z. Cai, T. Holmes, Y. Tao, *Chemosphere* **2017**, *186*, 977.

[39] L. A. Nirmal, R. Vishal, S. A. Bhakthochidan, V. B. Roshini, S. Jacob, *Int. J. Environ. Sci. Technol.* **2021**, *19*, 3015.

[40] Q. Wu, L. Guo, Y. Wang, Y. Zhao, C. Jin, M. Gao, Z. She, *Chemosphere* **2021**, *285*, 131366.

[41] K. Nobaharan, S. Bagheri Novair, B. Asgari Lajayer, E. van Hullebusch, *Water* **2021**, *13*, 517.

[42] K. Liu, J. Li, H. Qiao, A. Lin, G. Wang, *Bioresour. Technol.* **2012**, *114*, 26.

[43] A. Mohseni, M. Kube, L. Fan, F. A. Roddick, *Chemosphere* **2021**, *276*, 130028.

[44] J. M. Puguan, X. Yu, H. Kim, *J. Colloid Interface Sci.* **2014**, *432*, 109.

[45] K. Y. Lee, D. J. Mooney, *Prog. Polym. Sci.* **2012**, *37*, 106.

**ADVANCED
SCIENCE NEWS**

www.advancedsciencenews.com

**ADVANCED
ENERGY & SUSTAINABILITY
RESEARCH**
Open Access

www.advenergysustres.com

[46] M. N. Saqib, F. Liu, M. Chen, S. Ahammed, X. Liu, F. Zhong, *Food Hydrocolloids* **2022**, *131*, 107777.

[47] G. Ben Messaoud, L. Sanchez-Gonzalez, L. Probst, S. Desobry, *J. Colloid Interface Sci.* **2016**, *469*, 120.

[48] W. J. Duncanson, T. E. Kodger, S. Babaee, G. Gonzalez, D. A. Weitz, K. Bertoldi, *Langmuir* **2015**, *31*, 3489.

[49] M. Pereda, D. Poncelet, D. Renard, *Food Biophys.* **2019**, *14*, 467.

[50] M. H. Ghanian, H. Mirzadeh, H. Baharvand, *Biomacromolecules* **2018**, *19*, 1646.

[51] T. N. Cao, H. Mukhtar, L. T. Le, D. P. Tran, M. T. T. Ngo, M. D. Pham, T. B. Nguyen, T. K. Vo, X. T. Bui, *Sci. Total Environ.* **2023**, *870*, 161927.

[52] B. K. Gonzalez-Perez, A. M. Rivas-Castillo, A. Valdez-Calderon, M. A. Gayosso-Morales, *World J. Microbiol. Biotechnol.* **2021**, *38*, 4.